Optimal Renewable Energy Curtailment Minimization Control Using a Combined Electromobility and Grid Model

Mladen Čičić, Carlos Vivas, Carlos Canudas de Wit, Francisco Rubio

Optimal Renewable Energy Curtailment Minimization Control Using a Combined Electromobility and Grid Model

Mladen Čičić * **Carlos Vivas** ** **Carlos Canudas-de-Wit** * **Francisco R. Rubio** **

* *Univ. Grenoble Alpes, CNRS, Inria, Grenoble INP, GIPSA-lab, Grenoble, France*
** *Dept. de Ingeniería de Sistemas y Automática, Escuela Técnica Superior de Ingeniería, Universidad de Sevilla, Spain*

Abstract: In this paper we propose an integrated power and transportation system control framework, combining the power grid model with a macroscopic electromobility model including charging stations under V2G operation. In this framework, the electrical vehicles (EVs) act as energy storage, but also as an additional virtual power grid link, transporting energy from one point to another. This new holistic model is used as a basis for optimal control design seeking to minimize renewable energy curtailment, while accounting for the structural limitation of the grid and other SoC constraints necessary for the optimal operation of the EVs. The proposed control scheme is shown to eliminate approximately 50% of curtailment compared to uncoordinated EV charging.

Keywords: Electromobility, Optimal control, Renewable energy sources, Energy curtailment, Grid optimization

1. INTRODUCTION

As efforts towards decarbonization of all economical sectors become a major priority, Electric Vehicles (EVs) have started to emerge as one of the main components of sustainable transportation systems worldwide. Since EVs are projected to reach around 40% of the total fleet in the EU by 2030 (Conway et al., 2021), it is becoming clear that their integration with the city infrastructure (charging stations), and the electrical power supply network (power grid) poses unsolved problems that will be critical in the coming years (EU 2019).

Although the constant increase of the electrification of the transportation systems (*electromobility*) could be interpreted as a serious potential strain on the power grid due to the large charging power demands (Fernandez et al., 2010), the massive adoption of EVs will not necessarily hinder the development of future electric power systems. In fact, the potential to use their batteries for energy storage will help with the introduction of renewable energy sources (RES) (Wenzel et al., 2017) by increasing their dispatchability, making the EVs an important component of the power system operations. From the power system side, the grid can use this capacity to deal with network congestion management issues, as they can provide EV-flexibility (ability to quickly modify the demand to react to changing conditions), which is especially important in a foreseen future energy scenario dominated by intermittent RES. As the natural interface between the mobility and power networks, the charging stations will play an essential role in the electromobility ecosystem. Today's power electronics technology and new DC grid topologies, together with V2G-enabled EVs, allow charging stations to operate as dynamic load/supplies providing ancillary services to the power grid in the form of frequency stabilization and congestion relief López et al. (2013). Note that the EV flows on the roads can also be seen as additional virtual links in the power grid, which not only store energy but also carry energy from one point to another (a 3-lane highway with 25% of the traffic being EVs whose batteries have a capacity of 40 kWh is approximately equivalent to a 110 kV power line in terms of transported power!).

One of the main potential barriers to fully exploit the EVs' potential is the lack of tools and methods for forecasting EV fleets' flexibility in both time and space. This entails forecasting when and where EVs will move, how their State of Charge (SoC) will evolve, and how they will interact with the infrastructure. Though some approaches based on historical data do exist (Morlock et al., 2019), a model-based framework is preferable for optimal control purposes. Therefore, combining electromobility models with power grid models will enable the use of EVs' flexibility potential to minimize the RES curtailment and improve the use of the existing power transmission network. In Henry and Ernst (2021), RES curtailment was minimized by means of an optimal control strategy, which was also used to learn a computationally efficient control law based on reinforcement learning. Nevertheless, in this work storage and charging of EVs was assumed to be situated at a single point in the power network, whereas in reality both the EVs and the charging stations are distributed in

⋆ E-mail: mladen.cicic@gipsa-lab.fr, carlos.canudas-de-wit@cnrs.fr, vivas@us.es, rubio@us.es

time (in case of EVs) and space, and connected to different power grid nodes. In Zhou et al. (2021), coupled traffic and power grid dynamics were considered, but the traffic flows were only described on graph level.

In this paper we propose for the first time in the literature an integrated model, combining the power grid model with a macroscopic electromobility model distributed in space, including charging stations under V2G operation (in Section 2). The proposed multi-class electromobility model extends the simplified CTEC model previously proposed in Čičić and Canudas-de-Wit (2022) to capture a richer electromobility dynamics by allowing for several different co-located SoC levels in the vehicular flow. The electromobility layer is interfaced with the power layer through the charging stations, which act as predictable time-varying energy storage. This novel holistic model is used as a basis for optimal control design seeking to minimize RES curtailment, while accounting for the structural limitations of the grid and other SoC constraints necessary for the best possible operation of the EVs (in Section 3). Finally, the control framework is tested in simulations (in Section 4), based on which we are able to draw conclusions (in Section 5).

2. COMBINED ELECTROMOBILITY AND POWER GRID MODEL

In this section we present the combined electromobility and power grid model. We first introduce the new multi-class aggregated electromobility model including the charging stations, then we present the grid model, and finally connect the two parts into a combined model. The scenario studied in this work is similar to the one used in Henry and Ernst (2021), abstracting the situation where people commute between home and work using EVs, potentially stopping on the way at a public charging station. As shown in Fig. 1, we consider a power grid with three nodes (*Home*, *Public charging station*, and *Work*, in further text denoted by **h**, **p**, and **w**, respectively) connected both by power lines and road links. The two considered road links connect nodes **h** and **w**, with a pair of off- and on-ramps at the middle, exiting towards node **p**. We assume that there is intermittent RES power generation and EV charging ports at all three nodes, and that there is some time-varying load at nodes **h** and **w**. While the combined model is adapted to this specific setup it can accommodate other types of road and power networks as well.

2.1 Electromobility model

In this section we introduce a *multi-class* extension of the simplified CTEC model (Čičić and Canudas-de-Wit, 2022) to capture the electromobility dynamics. The model consists of the macroscopic dynamics of the EVs on the roads and the dynamics of the EVs at charging stations, coupled through ramp flows. In this work, we focus on the discretized version of the model, and the reader is referred to the cited paper for its continuous-time PDE version,

$$\frac{\partial \rho(x,t)}{\partial t} + \frac{\partial (v(x,t)\rho(x,t))}{\partial x} = 0, \tag{1}$$

$$\frac{\partial \varepsilon(x,t)}{\partial t} + v(x,t)\frac{\partial \varepsilon(x,t)}{\partial x} = \mathcal{D}(v(x,t)), \tag{2}$$

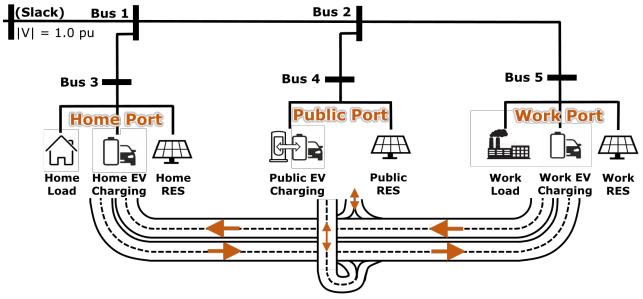

Fig. 1. Layout of the combined electromobility and power grid model used for this study.

$$\frac{\partial \eta(\varepsilon,t)}{\partial t} + \frac{\partial (c(\varepsilon,t)\eta(\varepsilon,t))}{\partial \varepsilon} = 0, \tag{3}$$

where x is the position along the road, t the time, $\rho(x,t)$ the traffic density, $v(x,t)$ the traffic speed, $\varepsilon(x,t)$ the SoC, $\mathcal{D}(v)$ the battery discharge as a function of EV speed, $\eta(\varepsilon,t)$ the distribution of EVs at a charging station according to their SoC ε, and $c(\varepsilon,t)$ the charging rate of EVs, potentially different for different ε. We extend the discretized version of the model by splitting the traffic flows into different classes which have the same behaviour while driving on the road, but may have independent SoC dynamics or behaviour at on- and off-ramps. These classes can be used to distinguish e.g. between combustion engine vehicles and EVs, or between vehicles with different routes and/or SoC, in order to avoid problems with the situation when two traffic flows with very different SoC merge.

Aggregate traffic density equations. Each road l is split into N_x^l cells of length L_x satisfying $L_x \geq v_{\text{ff}} T$, where v_{ff} is the free flow speed of the traffic, and T is the sampling period for electromobility model which need to be suitable selected to fulfil the numerical stability requirements. The aggregate macroscopic state of EV traffic on each road link l is given by the traffic density ρ_i^k and SoC ε_i^k in each cell i at each discrete time instant k. Since here we consider multiple classes of vehicles, the aggregate macroscopic SoC ε_i^k is not used, but instead we will track the SoC of each class. The update equations for the aggregate traffic density are:

$$\rho_i^{k+1} = \rho_i^k + \frac{T}{L_x}\left(q_{i-}^k - q_{i+}^k\right), \tag{4}$$

$$q_{i+}^k = \min\left\{ v_{\text{ff}}\underline{\rho}_i^k, \frac{\omega(\rho_{\text{jam}} - \overline{\rho}_{i+1}^k) - r_{\text{on},i+1}^k}{1-\beta_i^k} \right\}, \tag{5}$$

$$q_{i-}^k = q_{i-1+}^k(1-\beta_{i-1}^k) + r_{\text{on},i}^k, \tag{6}$$

Here, q_{i-}^k denotes the traffic flow entering cell i at its upstream end, and q_{i+}^k the traffic flow exiting cell i at its downstream end. The on-ramp flow into cell i is denoted $r_{\text{on},i}^k$ and assumed to enter it at its upstream end, and the off-ramp flow from cell i is assumed to leave it at its downstream end, and denoted $r_{\text{off},i}^k = \beta_i^k q_{i+}^k$, where β_i^k is the splitting ratio of mainstream traffic flow towards the off-ramp. The traffic is assumed to follow a triangular fundamental diagram with critical density ρ_{cr} and jam density ρ_{jam}, yielding congestion wave speed $\omega = v_{\text{ff}}\frac{\rho_{\text{cr}}}{\rho_{\text{jam}}-\rho_{\text{cr}}}$, and we denote $\underline{\rho}_i^k = \min\{\rho_i^k, \rho_{\text{cr}}\}$ and $\overline{\rho}_i^k = \max\{\rho_i^k, \rho_{\text{cr}}\}$. Note that we omit stating to which road link l we are referring for better readability.

Multi-class traffic density equations. The aggregate traffic flow may be split into some number of traffic classes $\xi \in \Xi$, with individual traffic densities denoted ${}^{\xi}\rho_i^k$. Since here we assume that all vehicle classes have the same behavior in traffic, the evolution of their traffic densities is given by

$$ {}^{\xi}\rho_i^{k+1} = {}^{\xi}\rho_i^k + \frac{T}{L_x}\left({}^{\xi}q_{i-}^k - {}^{\xi}q_{i+}^k\right), \tag{7} $$

$$ {}^{\xi}q_{i+}^k = \frac{{}^{\xi}\rho_i^k}{\rho_i^k} q_{i+}^k, \tag{8} $$

$$ {}^{\xi}q_{i-}^k = {}^{\xi}q_{i-1+}^k(1 - {}^{\xi}\beta_{i-1}^k) + {}^{\xi}r_{\mathrm{on},i}^k, \tag{9} $$

where the ramp flows defined through ${}^{\xi}\beta_{i-1}^k$ and ${}^{\xi}r_{\mathrm{on},i}^k$ are defined independently for each class ξ, with ${}^{\xi}r_{\mathrm{off},i}^k = {}^{\xi}\beta_{i-1}^k\, {}^{\xi}q_{i+}^k$. The per-class quantities relate to the aggregate quantities according to

$$ \rho_i^k = \sum_{\xi\in\Xi} {}^{\xi}\rho_i^k,\ r_{\mathrm{on},i}^k = \sum_{\xi\in\Xi} {}^{\xi}r_{\mathrm{on},i}^k,\ \beta_i^k = \sum_{\xi\in\Xi} \frac{{}^{\xi}\rho_i^k}{\rho_i^k}\, {}^{\xi}\beta_i^k. \tag{10} $$

Once the vehicles reach the end of the road link from **h** to **w** or from **w** to **h**, all of them exit the road and enter the respective charging station, $\beta_{N_x}^k = 1$ for both road links. The splitting ratios towards the public charging stations ${}^{\xi}\beta_i^k$, where $i = i_{\mathbf{ph}}^{\mathrm{in}}$ for the link **h** to **w**, and $i = i_{\mathbf{pw}}^{\mathrm{in}}$ for **w** to **h**, depend on the SoC of the approaching vehicles in the same cell i,

$$ {}^{\xi}\beta_i^k = 1 - \left(1 + e^{-\frac{{}^{\xi}\varepsilon_i^k - \varepsilon_{\mathrm{low}}}{\gamma}}\right)^{-1}, \tag{11} $$

as a monotonically decreasing sigmoid function centered at some $\varepsilon_{\mathrm{low}}$, with slope calibrated by some parameter γ. This function models the assumption that EVs are more likely to stop to charge if their SoC is low.

Multi-class SoC equations. The macroscopic SoC of each class is denoted ${}^{\xi}\varepsilon_i^k$, and its evolution is defined by

$$ {}^{\xi}\rho_i^{k+1}\,{}^{\xi}\varepsilon_i^{k+1} = {}^{\xi}\rho_i^k\left({}^{\xi}\varepsilon_i^k + {}^{\xi}d_i^k T\right) + \frac{T}{L_x}\left({}^{\xi}\phi_{i-}^k - {}^{\xi}\phi_{i+}^k\right), \tag{12} $$

$$ {}^{\xi}\phi_{i-}^k = ({}^{\xi}q_{i-}^k - {}^{\xi}r_{\mathrm{on},i}^k)\left({}^{\xi}\varepsilon_{i-1}^k + {}^{\xi}d_{i-1}^k T\right) + {}^{\xi}r_{\mathrm{on},i}^k\, {}^{\xi}\varepsilon_{\mathrm{on},i}^k, \tag{13} $$

$$ {}^{\xi}\phi_{i+}^k = {}^{\xi}q_{i+}^k\left({}^{\xi}\varepsilon_i^k + {}^{\xi}d_i^k T\right). \tag{14} $$

where the battery discharge rate ${}^{\xi}d_i^k$ depends on the traffic speed in cell i,

$$ {}^{\xi}d_i^k = \mathcal{D}_{\xi}\left(v_i^k\right), \quad v_i^k = \frac{q_{i+}^k}{\rho_i^k}, \tag{15} $$

and is defined by potentially different discharge functions for each class $\mathcal{D}_{\xi}$.

Charging stations equations. Finally, the electromobility model is completed by the charging station dynamics. For each charging station ζ, we split the SoC space into N_ε bins of length L_ε, $N_\varepsilon L_\varepsilon = 1$. Each bin $j = 1, \ldots, N_\varepsilon$ corresponds to a range of SoC $[(j-1)L_\varepsilon, jL_\varepsilon]$, and we describe the state of the charging station through the number of vehicles in each bin ${}^{\zeta}\eta_j^k$.

Different classes of vehicles at a single physical charging station can be represented by using multiple virtual charging stations ζ to represent charging of each vehicle class ξ. We allow the rate of charging ${}^{\zeta}c_j^k$ for each charging station ζ and for each SoC level j, to vary in time within some range $\left|{}^{\zeta}c_j^k\right| \le C$, with $L_\varepsilon \ge CT$ required for numeric stability. The charging station state update is then given by

$$ \begin{aligned} {}^{\zeta}\eta_j^{k+1} = {}^{\zeta}\eta_j^k + \frac{T}{L_\varepsilon}\big({}^{\zeta}\underline{c}_{j-1}^k\, {}^{\zeta}\eta_{j-1}^k - \left|{}^{\zeta}c_j^k\right|{}^{\zeta}\eta_j^k - {}^{\zeta}\overline{c}_{j+1}^k\, \eta_{j+1}^k\big)\ldots \\ \ldots + T\big({}^{\zeta}\mu_{\mathrm{in},j}^k - {}^{\zeta}\mu_{\mathrm{out},j}^k\big), \end{aligned} \tag{16} $$

where ${}^{\zeta}\underline{c}_j^k = \max\{0, {}^{\zeta}c_j^k\}$, and ${}^{\zeta}\overline{c}_j^k = \min\{0, {}^{\zeta}c_j^k\}$, and ${}^{\zeta}\mu_{\mathrm{in},j}^k$ and ${}^{\zeta}\mu_{\mathrm{out},j}^k$ represent the flows of vehicles entering and exiting the charging station, respectively.

The flows between the road and the charging station ζ are

$$ r_{\mathrm{on},i_\zeta^{\mathrm{out}}}^k = \sum_{j=1}^{N_\varepsilon} {}^{\zeta}\mu_{\mathrm{out},j}^k,\ r_{\mathrm{on},i_\zeta^{\mathrm{out}}}^k \varepsilon_{\mathrm{on},i_\zeta^{\mathrm{out}}}^k = \sum_{j=1}^{N_\varepsilon} {}^{\zeta}\mu_{\mathrm{out},j}^k (j-1)L_\varepsilon, \tag{17} $$

$$ r_{\mathrm{off},i_\zeta^{\mathrm{in}}}^k = \sum_{j=1}^{N_\varepsilon} {}^{\zeta}\mu_{\mathrm{in},j}^k, \qquad r_{\mathrm{off},i_\zeta^{\mathrm{in}}}^k \varepsilon_{i_\zeta^{\mathrm{in}}}^k = \sum_{j=1}^{N_\varepsilon} {}^{\zeta}\mu_{\mathrm{in},j}^k (j-1)L_\varepsilon, \tag{18} $$

where i_ζ^{in} and i_ζ^{out} are the cells where the off- and on-ramp connecting the road to the charging station ζ are, respectively, ensuring both the vehicles and the energy are conserved. In this work, we assume that multiple classes of vehicles can enter a single charging station ζ,

$$ {}^{\zeta}\mu_{\mathrm{in},j}^k = \sum_{\xi\in\Xi} {}^{\zeta,\xi}\mu_{\mathrm{in},j}^k, \tag{19} $$

and that all vehicles exiting the charging station are of the same class ξ_ζ^{out}, therefore ${}^{\xi}r_{\mathrm{on},i_\zeta^{\mathrm{out}}}^k = r_{\mathrm{on},i_\zeta^{\mathrm{out}}}^k$ with $\xi = \xi_\zeta^{\mathrm{out}}$, and ${}^{\xi}r_{\mathrm{on},i_\zeta^{\mathrm{out}}}^k = 0$ for $\xi \ne \xi_\zeta^{\mathrm{out}}$. The flows entering and exiting the charging stations are further determined by

$$ {}^{\zeta,\xi}\mu_{\mathrm{in},j}^k = \begin{cases} \left(j - \dfrac{{}^{\xi}\varepsilon_{i_\zeta^{\mathrm{in}}}^k}{L_\varepsilon}\right){}^{\xi}r_{\mathrm{off},i_\zeta^{\mathrm{in}}}^k, & j-1 \le \dfrac{{}^{\xi}\varepsilon_{i_\zeta^{\mathrm{in}}}^k}{L_\varepsilon} < j, \xi \in \Xi_\zeta^{\mathrm{in}}, \\ \left(\dfrac{{}^{\xi}\varepsilon_{i_\zeta^{\mathrm{in}}}^k}{L_\varepsilon} - j + 2\right){}^{\xi}r_{\mathrm{off},i_\zeta^{\mathrm{in}}}^k, & j-2 \le \dfrac{{}^{\xi}\varepsilon_{i_\zeta^{\mathrm{in}}}^k}{L_\varepsilon} < j-1, \xi \in \Xi_\zeta^{\mathrm{in}}, \\ 0, & \text{otherwise}, \end{cases} \tag{20} $$

$$ {}^{\zeta}\mu_{\mathrm{out},j}^k \in \left[0, \left(\frac{1}{T} - \frac{\left|{}^{\zeta}c_j^k\right|}{L_\varepsilon}\right){}^{\zeta}\eta_j^k + \frac{{}^{\zeta}\underline{c}_{j-1}^k}{L_\varepsilon}{}^{\zeta}\eta_{j-1}^k - \frac{{}^{\zeta}\overline{c}_{j+1}^k}{L_\varepsilon}{}^{\zeta}\eta_{j+1}^k\right], \tag{21} $$

where Ξ_ζ^{in} denotes the set of vehicle classes that enter charging station ζ, and the exiting flow ${}^{\zeta}\mu_{\mathrm{out},j}^k$ depends on the particular behavioural logic of each charging station. We assume that each traffic class ξ enters at most one charging station ζ from each cell i, but it may enter multiple charging stations in case off-ramps leading to them are in different cells $i_{\zeta_1}^{\mathrm{in}} \ne i_{\zeta_2}^{\mathrm{in}}$.

Charging stations control variables. Charging stations are of particular importance because they serve as the interface between the electromobility layer and the power grid, and can be used as actuators to improve the situation in the wider power system. At each time step k, the power system operator gets from each charging station ζ the range of power that they can consume or generate, denoted by $\overline{U}_\zeta^k$ and $\underline{U}_\zeta^k$, respectively. Based on these limits, the operator can choose the normalized current power flow to (or from) each charging station ζ, denoted $u_\zeta^k \in [-1, 1]$. Here we adopt the convention that if $u_\zeta^k > 0$, the charging

station is a net power consumer from the perspective of the grid, and is using the grid power to charge the EVs. Otherwise, if $u_\zeta^k < 0$, the charging station is a net power provider to the grid, and is using the energy stored in the batteries of some EVs to provide V2G services. The actual charging station powers, denoted U_ζ^k, represent the control input to the electromobility system, and are given by

$$U_\zeta^k = \begin{cases} u_\zeta^k \overline{U}_\zeta^k, & u_\zeta^k \geq 0, \\ u_\zeta^k \underline{U}_\zeta^k, & u_\zeta^k < 0, \end{cases} \tag{22}$$

therefore we have $\underline{U}_\zeta^k \leq U_\zeta^k \leq \overline{U}_\zeta^k$. This charging station power relates to its EV charging rates as

$$U_\zeta^k = \sum_{j=1}^{N_\varepsilon} {}^\zeta c_j^k \, {}^\zeta\eta_j^k B \tag{23}$$

where B is the EV battery average capacity. In order to best utilize the available power, we employ a hierarchical charging scheme, where vehicles with lower SoC have a higher priority for charging. We split the vehicles into three groups according to their SoC: low SoC EVs, with $0 \leq \varepsilon < \varepsilon_{\text{low}}$, medium SoC EVs, with $\varepsilon_{\text{low}} \leq \varepsilon \leq \varepsilon_{\text{high}}$, and high SoC EVs, with $\varepsilon_{\text{high}} < \varepsilon \leq 1$. Additionally, in case there is not enough power to charge the low SoC EVs, as well as if the grid operators requests power to be provided to the grid, we utilize the energy stored in batteries of EVs with higher SoC, discharging their batteries to satisfy the power demands.

Given the boundaries between these groups of EVs ε_{low} and $\varepsilon_{\text{high}}$, we define j_{low} as the highest j for which $\varepsilon_j < \varepsilon_{\text{low}}$ and j_{high} as the lowest for which $\varepsilon_j > \varepsilon_{\text{high}}$, $j \in \{1, \ldots, N_\varepsilon\}$. The number of EVs currently in each group is defined by

$${}^\zeta\eta_{\text{low}}^k = \sum_{j=1}^{j_{\text{low}}} {}^\zeta\eta_j^k, \;\; {}^\zeta\eta_{\text{med}}^k = \sum_{j=j_{\text{low}}+1}^{j_{\text{high}}-1} {}^\zeta\eta_j^k, \;\; {}^\zeta\eta_{\text{high}}^k = \sum_{j=j_{\text{high}}}^{N_\varepsilon} {}^\zeta\eta_j^k. \tag{24}$$

For each charging station we define the maximum charging rate $C_\zeta^{\max} \geq 0$ and maximum discharging rate $C_\zeta^{\min} \leq 0$ per EV, yielding $C_\zeta^{\min} \leq {}^\zeta c_j^k \leq C_\zeta^{\max}$, respecting $|C_\zeta^{\max}| \leq C$ and $|C_\zeta^{\min}| \leq C$. We assign a different charging rate to each group of EVs, denoted ${}^\zeta c_{\text{low}}^k$, ${}^\zeta c_{\text{med}}^k$, and ${}^\zeta c_{\text{high}}^k$, and given by

$${}^\zeta c_j^k = \begin{cases} {}^\zeta c_{\text{low}}^k, & j = 1, \ldots, j_{\text{low}}, \\ {}^\zeta c_{\text{med}}^k, & j = j_{\text{low}}+1, \ldots, j_{\text{high}}-1, \\ {}^\zeta c_{\text{high}}^k, & j = j_{\text{high}}, \ldots, N_\varepsilon. \end{cases} \tag{25}$$

The exception is charging at home, $\zeta = \text{h}$, where we assume that all vehicles charge at the same rate,

$${}^{\text{h}}c_j^k = \min\left\{ \frac{P_{\text{h}}^k}{{}^{\text{h}}\eta_{\text{low}}^k + {}^{\text{h}}\eta_{\text{med}}^k + {}^{\text{h}}\eta_{\text{high}}^k}, C_{\text{h}}^{\max} \right\}. \tag{26}$$

Given the current provided or demanded power U_ζ^k, these charging rates are given by

$${}^\zeta c_{\text{low}}^k = \min\left\{ \frac{{}^\zeta\mathcal{P}_{\text{low}}^k}{{}^\zeta\eta_{\text{low}}^k}, C_\zeta^{\max} \right\}, \tag{27}$$

$${}^\zeta c_{\text{med}}^k = \begin{cases} C_\zeta^{\min}, & {}^\zeta\eta_{\text{low}}^k C_\zeta^{\max} > {}^\zeta\mathcal{P}_{\text{low}}^k, \\ \min\left\{ \dfrac{{}^\zeta\mathcal{P}_{\text{med}}^k}{{}^\zeta\eta_{\text{med}}^k}, C_\zeta^{\max} \right\}, & {}^\zeta\eta_{\text{low}}^k C_\zeta^{\max} \leq {}^\zeta\mathcal{P}_{\text{low}}^k, \end{cases} \tag{28}$$

$${}^\zeta c_{\text{high}}^k = \begin{cases} C_\zeta^{\min}, & {}^\zeta\eta_{\text{med}}^k C_\zeta^{\max} > {}^\zeta\mathcal{P}_{\text{med}}^k, \\ \min\left\{ \dfrac{{}^\zeta\mathcal{P}_{\text{high}}^k}{{}^\zeta\eta_{\text{med}}^k}, C_\zeta^{\max} \right\}, & {}^\zeta\eta_{\text{med}}^k C_\zeta^{\max} \leq {}^\zeta\mathcal{P}_{\text{med}}^k, \end{cases} \tag{29}$$

where we define maximum available charging power to each group of vehicles, ${}^\zeta\mathcal{P}_{\text{low}}^k$, ${}^\zeta\mathcal{P}_{\text{med}}^k$, and ${}^\zeta\mathcal{P}_{\text{high}}^k$, as

$${}^\zeta\mathcal{P}_{\text{low}}^k = U_\zeta^k - \left({}^\zeta\eta_{\text{med}}^k + {}^\zeta\eta_{\text{high}}^k\right) C_\zeta^{\min}, \tag{30}$$

$${}^\zeta\mathcal{P}_{\text{med}}^k = U_\zeta^k - {}^\zeta\eta_{\text{med}}^k C_\zeta^{\max} - {}^\zeta\eta_{\text{high}}^k C_\zeta^{\min}, \tag{31}$$

$${}^\zeta\mathcal{P}_{\text{high}}^k = U_\zeta^k - {}^\zeta\eta_{\text{high}}^k C_\zeta^{\max}. \tag{32}$$

Finally, the presented charging scheme results in a range of power that charging station ζ can consume or produce $[\underline{U}_\zeta^k, \overline{U}_\zeta^k]$ given by

$$\overline{U}_\zeta^k = \left({}^\zeta\eta_{\text{low}}^k + {}^\zeta\eta_{\text{med}}^k + {}^\zeta\eta_{\text{high}}^k\right) C_\zeta^{\max} B, \tag{33}$$

$$\underline{U}_\zeta^k = \max\left\{0, \left({}^\zeta\eta_{\text{low}}^k C_\zeta^{\max} + \left({}^\zeta\eta_{\text{med}}^k + {}^\zeta\eta_{\text{high}}^k\right) C_\zeta^{\min} \, {}^\zeta\eta_j^k\right) B\right\}. \tag{34}$$

Finally, we define the flows of EVs exiting each charging stations according to their scheduled departure demand function ${}^\zeta\hat{\mu}_{\text{out}}^k$,

$${}^\zeta\mu_{\text{out},j}^k = \begin{cases} \min\left\{ {}^\zeta\hat{\mu}_{\text{out}}^k, \left(\frac{1}{T} - \frac{|{}^\zeta c_j^k|}{K_\varepsilon}\right) {}^\zeta\eta_j^k \right\}, & j = j_\zeta^k, \\ 0, & j \neq j_\zeta^k. \end{cases} \tag{35}$$

For $\zeta = \mathbf{h}$ and $\zeta = \mathbf{w}$, ${}^\zeta\hat{\mu}_{\text{out}}^k$ is given externally, to represent EVs commuting from home around $t = 6$ h, and from work to home around $t = 16$ h. For $\zeta = \mathbf{p}$, we assume that the EVs stay at the charging station for 1 h, so the departure demand will depend on the flow entering the charging station in the past. At each sampling time, we randomly select the SoC of the departing EVs for each charging station j_ζ^k, with probabilities of each SoC level proportional to the number of vehicles currently at charging station ζ.

2.2 Power Grid Model

This section describes the dynamics of the alternating current (AC) power grid that is employed to model the interaction between a conventional grid and the electromobility layer. To avoid confusion regarding notation conventions, and reduce abuse of notation, we indicate the parameters and variables of the power grid model by tilde.

Nowadays, the vast majority of AC transmission and distribution networks dispatch electricity using a three-phase system. Three parallel circuits are employed, each associated with its own phase, shifted 120^o from one another. Balanced three-phase system can be represented in phasor form as an equivalent single-phase representation, where only one of the phases is taken into account. In this work, power transmission lines are assumed to constitute such three-phase balanced networks, and we adopt its equivalent single-phase representation in the following derivations. Also, for mathematical convenience, the power system will be analyzed using the per-unit (p.u.) notation, in which all electrical quantities are normalized with respect to a set of base quantities. This normalization approach is widely used as it removes the need to include nominal voltage levels in derivations.

The distribution grid is modelled as a set of nodes $\tilde{\mathcal{N}}$ linked by a set of directed edges $\tilde{\mathcal{E}}$ that represent the transmission lines. Each edge $\tilde{e}_{ij} \in \tilde{\mathcal{E}}$ links buses i and j and can contain transmission lines, power transformers and/or phase shifters. Here the conventional π transmission line model is employed where each branch can be defined by five parameters: a series resistance $\tilde{r}_{ij}$, a series reactance $\tilde{x}_{ij}$, a charging susceptance $\tilde{b}_{ij}$, a tap ratio magnitude $\tilde{\tau}_{ij}$ and phase shift $\tilde{\theta}_{ij}$. These magnitudes allows to define the link series admittance $\tilde{y}_{ij} = 1/(\tilde{r}_{ij} + \sqrt{-1}\tilde{x}_{ij})$ and shunt admittance $\tilde{y}^{\text{sh}}_{ij} = \sqrt{-1}\frac{\tilde{b}_{ij}}{2}$ as well as the complex tap ratio of transformers, $\tilde{t}_{ij} = \tilde{\tau}_{ij}e^{\sqrt{-1}\tilde{\theta}_{ij}}$. See Zimmerman et al. (2011) for a more detailed explanation of the branch convention employed.

Power Network equations. For a network with $\tilde{N}_{\text{b}} = |\tilde{\mathcal{N}}|$ buses, and after applying Kirchhoff's current law at each bus $i \in \tilde{\mathcal{N}}$, the constant impedance elements of the model are incorporated into a complex $\tilde{N}_{\text{b}} \times \tilde{N}_{\text{b}}$ bus admittance matrix $\tilde{Y}$ that relates the complex nodal current injections, $\tilde{I}$ to the complex node voltages, $\tilde{V}$, as $\tilde{I} = \tilde{Y}\tilde{V}$.

The impedance matrix admits a systematic definition as

$$\tilde{Y}_{ij} = \begin{cases} -\dfrac{\tilde{y}_{ij}}{\tilde{t}^*_{ij}}, & i \neq j, \tilde{e}_{ij} \in \tilde{\mathcal{E}}, \\ -\dfrac{\tilde{y}_{ij}}{\tilde{t}_{ij}}, & i \neq j, \tilde{e}_{ji} \in \tilde{\mathcal{E}}, \\ \displaystyle\sum_{\tilde{e}_{ik} \in \tilde{\mathcal{E}}} \frac{\tilde{y}_{ik} + \tilde{y}^{\text{sh}}_{ik}}{\tilde{t}_{ik}\tilde{t}^*_{ik}} + \sum_{\tilde{e}_{ki} \in \tilde{\mathcal{E}}} \tilde{y}_{ki} + \tilde{y}^{\text{sh}}_{ki}, & i = j, \\ 0, & \text{otherwise.} \end{cases}$$

Power flow solution. The standard power flow or load flow problem involves solving for the set of voltages and flows in a network corresponding to a specified pattern of load and generation. The definition of grid admittance matrix $\tilde{Y}$ allows to define the nodal equation in an equivalent form in terms of power injections and voltage level at buses as

$$\tilde{S}^{\text{bus}}_i = \tilde{V}_i\tilde{I}^*_i = \tilde{V}_i(\tilde{Y}_i\tilde{V})^* = \tilde{V}_i\tilde{Y}^*_i\tilde{V}^*, \quad \forall i \in \tilde{\mathcal{N}}, \tag{36}$$

where $\tilde{S}^{\text{bus}}_i = \tilde{P}^{\text{bus}}_i + \sqrt{-1}\tilde{Q}^{\text{bus}}_i$ is the complex power phasor accounting for active ($\tilde{P}^{\text{bus}}_i$) and reactive ($\tilde{Q}^{\text{bus}}_i$) powers injected at bus i, and $\tilde{Y}_i$ denotes the i-th row of the admittance matrix $\tilde{Y}$.

Equation (36) is a set of $\tilde{N}_{\text{b}}$ complex-valued equations, that can be posed as $2\tilde{N}_{\text{b}}$ quadratic real valued equations with $2\tilde{N}_{\text{b}}$ real unknowns. By convention, a single generator bus is typically chosen as a reference bus to serve the roles of both a voltage angle reference and a real power slack. The voltage angle at the reference bus has a known value, but the real power generation at the slack bus is taken as unknown to avoid overspecifying the problem. Unknowns for the problem will thus be active and reactive powers at the slack bus together with complex voltage level at the remaining $\tilde{N}_{\text{b}} - 1$ buses.

These equations are solved at every iterations step of the problem providing equilibrium powers and voltages at the bus level. The solver of choice employed in this work is based on a standard Newton's method Tinney and Hart (1967) using a polar form and a full Jacobian updated at each iteration. Each Newton step involves computing the mismatch, forming the Jacobian based on the sensitivities of these mismatches to changes in and solving for an updated value of the unknowns by factorizing this Jacobian.

2.3 Combined model

We denote the encapsulated full state of the mobility model at time k as E^k,

$$\begin{aligned} E^k = \Big(& {}^{\xi}\rho^k_{l,i} | l \in \{\mathbf{hw}, \mathbf{wh}\}, i = \{1, \dots, N_x\}, \xi \in \{\mathbf{h/w}, \mathbf{p}\}, \dots \\ & {}^{\xi}\varepsilon^k_{l,i} | l \in \{\mathbf{hw}, \mathbf{wh}\}, i = 1, \dots, N_x, \xi \in \{\mathbf{h/w}, \mathbf{p}\}, \dots \\ & {}^{\zeta}\eta^k_j | j \in \{1, \dots, N_\varepsilon\}, \zeta \in \{\mathbf{h}, \mathbf{w}, \mathbf{phw}, \mathbf{pwh}\} \Big), \end{aligned} \tag{37}$$

capturing the traffic density ${}^{\xi}\rho^k_{l,i}$ and SoC ${}^{\xi}\varepsilon^k_{l,i}$ for all vehicle classes ξ and all cells i on both road links l, and the numbers of charging vehicles ${}^{\zeta}\eta^k_j$ at each SoC level j at each charging station ζ. The vehicles are split into classes based on whether they enter the road from **h** or **w** (**h/w**), or from **p**. Physical charging station **p** is modelled by two virtual charging stations **pwm** and **phw**, based on what link it is connected to.

The electromobility state is updated according to (7), (12), and (16), as defined in Section 2.1, and we write jointly

$$E^{k+1} = \mathcal{M}(E^k, U^k), \tag{38}$$

where U^k is the collection of U^k_ζ to all physical charging stations, $\zeta \in \{\mathbf{h}, \mathbf{w}, \mathbf{p}\}$, yielding charging rates (25) that directly determine the evolution of ${}^{\zeta}\eta^k_j$ through (16).

Power grid equations at discrete time step k is given by a static mapping, and can be expressed compactly as

$$\tilde{F}^k = \tilde{\mathcal{F}}(U^k, \tilde{\Lambda}^k, \tilde{V}^k), \tag{39}$$

$$\tilde{P}^k_{\text{c}} = \tilde{\mathcal{C}}(\tilde{F}^k, \tilde{V}^k), \tag{40}$$

$$\tilde{P}^k_{\text{r}} = \tilde{\mathcal{R}}(E^k), \tag{41}$$

where $\tilde{F}^k$ are the power flows at time k as a function of the EV power injected/retrieved U^k, loads $\tilde{\Lambda}^k$, and RES distributed generation $\tilde{V}^k$. RES curtailment is is given by $\tilde{P}^k_{\text{c}}$, and mobility power reserves by $\tilde{P}^k_{\text{r},\zeta}$. Except for power flows $\tilde{F}^k$, all other variables in (39)–(41) are collection of variables related to different ports $\zeta \in \{\mathbf{h}, \mathbf{w}, \mathbf{p}\}$.

3. OPTIMAL CONTROL DESIGN

3.1 Power system optimization

Active network management (ANM) refers in the power system literature to the decision-making procedures to design control schemes that modulate loads, generators, and the distributed energy resources connected to the grid, in order to keep power grid operation within nominal conditions in terms of bus voltages, stable frequency and power lines capacities.

The modulation resulting from ANM often causes a necessary reduction in the output of generators from what they could otherwise have produced given available resources,

often referred to as the process of curtailment. Such generation curtailment, along with storage and transmission losses, constitute a major source of energy management inefficiencies that this work aims to improve. In addition, the ANM scheme must ensure a safe and reliable operation of the distribution network, expressed as a set of technical and operational constraints that must be satisfied.

The proposed optimization problem focuses on the reduction of curtailments by providing near future scheduling of the optimal power flow policy to/from EVs plugged at the different charging poles of the system (**h**, **w**, and **p**). This separation is designed to collect the spatiotemporal operation of a large majority of EV users commuting daily from home to work, and occasionally making use of public charging stations facilities.

The optimization problem is formulated based on a prediction model and operated in a receding horizon manner using the latest system information. In this approach, load injections and generation profiles of RES are non-controllable variables. Only the active power (and reactive, within operational limits) of EV demand is assumed to be manageable. The objective function, constraints, and optimization algorithm will be presented next.

3.2 Optimal control formulation

We can now formulate ANM taking electromobility into account as a receding horizon optimal control problem

$$\underset{\tilde{u}_\zeta^{\tilde{k}}}{\text{minimize}}\ J(\tilde{k}, \tilde{u}_\zeta^{\tilde{k}})$$

subject to Mobility and grid dynamics (38)-(41),
Grid operational constraints,

$$|\tilde{S}_{ij}| \leq \overline{\tilde{S}}_{ij}, \quad \tilde{e}_{ij} \in \tilde{\mathcal{E}}, \tag{42}$$

$$\underline{\tilde{V}}_i \leq \tilde{V}_i \leq \overline{\tilde{V}}_i, \quad i \in \tilde{\mathcal{N}} - \tilde{\mathcal{N}}_{\text{slack}}, \tag{43}$$

Reactive to active power ratio limitations.

The optimization problem is articulated as constrained minimization of the cost function

$$J(\tilde{k},\tilde{u}_\zeta^{\tilde{k}}) = \sum_{h=1}^{H} \sum_{\zeta \in \{\mathbf{h},\mathbf{p},\mathbf{w}\}} \left(w_{\text{c}} \tilde{P}_{\text{c},\zeta}(t_{\tilde{k}+h}|t_{\tilde{k}}) - w_{\text{r}} \tilde{P}_{\text{r},\zeta}(t_{\tilde{k}+h}|t_{\tilde{k}}) \right) \tag{44}$$

where $\tilde{P}_{\text{c},\zeta}(t_{\tilde{k}+h}|t_{\tilde{k}})$ represent the curtailed power at time $t_{\tilde{k}+h}$ inferred from the information available at time $t_{\tilde{k}}$, at port ζ. Similarly $\tilde{P}_{\text{r},\zeta}(t_{\tilde{k}+h}|t_{\tilde{k}})$ accounts for the mobility reserve power available at time $t_{\tilde{k}+h}$. Constants w_{c} and w_{r} weigh the different optimization terms. The optimization problem is subject to constraints on the maximum apparent power $|\tilde{S}_{ij}|$ (42), power line voltage $\tilde{V}_i$ deviation at buses (43), and limitations on the amount of reactive to active power ratios the distributed generation can manage.

Note that in order to ease the numeric burden, we solve this problem at a time scale different than that of the electromobility model. We take the optimization sampling period $\tilde{T}$ as a multiple of electromobility sampling periods T, and denote the optimization time step $\tilde{k}$. The resulting control $\tilde{u}_\zeta^{\tilde{k}}$ is then applied to the electromobility model over a number of time steps,

$$u_\zeta^k = \tilde{u}_\zeta^{\lfloor k \frac{T}{\tilde{T}} \rfloor + 1}, \tag{45}$$

where $\lfloor \cdot \rfloor$ denotes rounding down.

The first part of the cost function accounts for the overall energy that is lost in the system as a result of necessary curtailment imposed by the ANM algorithm to satisfy grid constraints for a predicted sequence of control actions $\tilde{u}_\zeta(t_{k+h}|t_k)$, $\zeta \in \{\mathbf{h}, \mathbf{p}, \mathbf{w}\}$, $h =, 1..., N_u$. The control actions correspond to the normalized active power that the controller schedules to be retrieved or injected (V2G) at port ζ, and N_u is the control horizon considered. In this scheme, as is usually employed in the classic formulation of predictive control, for $N_u > 1$ only the first control action of the sequence computed is applied. The control action terms $\tilde{u}_\zeta(t_{k+h}|t_k) \in [-1, 1]$ are considered in a normalized fashion, allowing to accommodate the constraints on the time-varying mobility reserve powers in a more convenient form. The second term is designed to maximize the mobility reserve storage available within the prediction horizon, which is taken for simplicity as a proxy of the overall SoC of the EV fleet.

4. SIMULATION RESULTS

Finally, we assess the behaviour of the proposed ANM EV charging scheme by comparing two simulation scenarios. The first one corresponds to uncoordinated charging where a fixed percentage of EVs at each charging station ζ is charging at constant maximum rate $C_\zeta^{\max}$. We set these percentages to 70% for $\zeta = \mathbf{h}$, and 40% for $\zeta = \mathbf{w}$ and $\zeta = \mathbf{p}$. The second scenario corresponds to a scheduled charging operation as proposed in this work using a receding horizon control scheme that balances curtailment losses in relation to average EV reserves. Note that in both cases vehicles decide whether or not they enter the public charging station depending on their SoC, according to (11). Algorithm 1 outlines the main steps to perform the proposed simulations and control design approach. Dynamic equations have been discretized to be approximated by a conventional fixed-step iteration algorithm.

Both scenarios have been simulated on the test layout described in Fig.1 where for the sake of simplicity, the power network is reduced to three representative ports that lump loads, distributed generation and EV operation for aggregated domestic, work and public EV charging stations. Simulations were performed assuming a grid configuration with balanced capacities on the three ports in the order of 30 MW. Power lines capacities were assigned

Algorithm 1 Sketched simulation algorithm

```
procedure GridMobSimulation
    Grid parameters Initialization
    Mobility subsystem parameter Initialization
    k̃ = 1
    while k̃ ≤ k̃_end do                    ▷ Simulation Loop
        P̃_r ← Get Mobility Reserves (Ẽ^k̃)
        ũ^k̃ ← Optimize for horizon H (P̃_r)
        Ẽ^{k̃+1} ← Update Mobility Model(ũ^k̃)
        Solve Instant Power Flow Balance (ũ^k̃)
        k̃ ← k̃ + 1
```

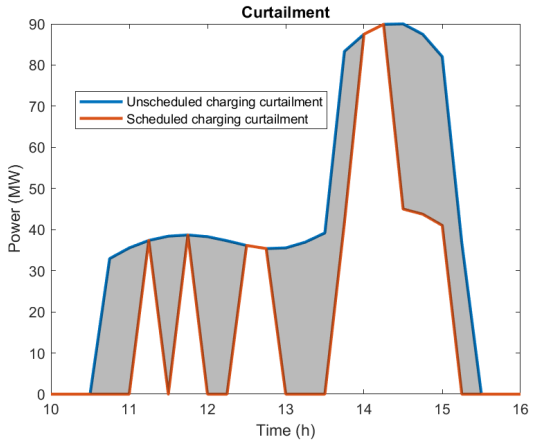

Fig. 2. Curtailment cut. Uncoordinated vs coordinated charging scenario

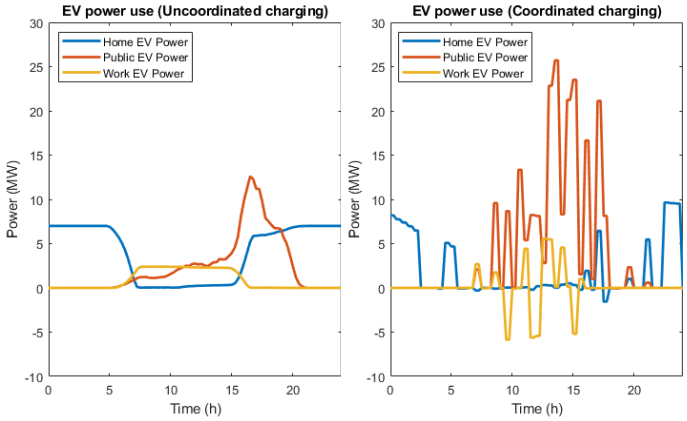

Fig. 3. EV power user for uncoordinated (left) and coordinated (right) scenarios.

to naturally induce RES curtailment at specific times of the day with high RES production and lower loads. Domestic and work loads, together with RES production have been simulated taking averaged typical profiles for every category. From the mobility side, a baseline of 3334 EVs with an average battery capacity of 60 kWh were considered, and their SoC was initialized in the $\varepsilon \in [0.5, 1]$ range.

Due to the daily cyclic nature of power loads, RES production and mobility patterns, simulations for a period of 24h were considered representative of the system. For the computation of the coordinated charging schedule, we used a prediction horizon of $H\tilde{T} = 5$ h, and a control horizon of $N_u\tilde{T} = 30$ min. To speed up computations, simulations were performed with different sample times, with $T = 1$ min for the electromobility model, 5 min for the power grid model and $\tilde{T} = 30$ min as sample time for the receding horizon control.

As a primary objective of the optimization problem proposed, the performance index in (44) has been balanced to maximize the use of RES (reduce curtailment losses), while preserving a reasonable average state of charge of the EVs. Figure 2 plots the compared curtailment induced by the uncoordinated and coordinated schemes, the shaded area corresponding to curtailment energy saving by the later approach. More precisely, in this particular simulation, the uncoordinated charging scenario induces 249.7 MWh losses in curtailment, while the coordinated approach provides 124.1 MWh, a significant reduction of 50.3%.

Figure 3 shows the evolution of the power used by EVs. For the uncoordinated charging scenario, the power used for charging is directly proportional to the number of EVs currently present at the charging station. Coordinated charging allows for a more nuanced use of power depending on the power grid load and RES production at different times of the day.

In order to illustrate the state of the electromobility model, we show the state of charging stations over time in Figure 4. As expected, all EVs start at home, then travel to work, and finally return home, with some of them stopping at the public charging station along the way. In this case EVs end the day with somewhat lower SoC, which will be rectified through overnight charging at home.

5. CONCLUSIONS

In this work, we present a control framework combining electromobility and the power grid. Using an extended multi-class electromobility model, we are able to capture the SoC dynamics of EVs on their daily commute. The electromobility layer is interfaced with the power grid through charging stations, providing us with a way to store energy and control the power flows. We use this framework to design a receding horizon control law for for active network management, in order to reduce RES production curtailment, which is shown in simulation to significantly improve the situation.

The models and results presented herein could serve as a basis for a number of future research directions. Though the network studied here was adopted for simplicity, the presented control approach should be extended to a more general case and more complex networks, both in terms of roads and power lines. In this work, we did not utilize the ratio of EVs that enter the public charging station as a control input, but this behavior could be influenced by e.g. introducing dynamic pricing of charging, which opens an entirely new area of control problems.

ACKNOWLEDGEMENTS

This work has received support from the Scale-FreeBack project, funding by the European Research Council (ERC) under the European Union's Horizon 2020 research and innovation programme (grant agreement N 694209), and by projects PID2020-115561RB-C32 granted by the Spanish Ministry of Science and Innovation.

REFERENCES

Čičić, M. and Canudas-de-Wit, C. (2022). Coupled macroscopic modelling of electric vehicle traffic and energy flows for electromobility control. In *CDC 2022-61st IEEE Conference on Decision and Control.*

Conway, G., Joshi, A., Leach, F., García, A., and Senecal, P.K. (2021). A review of current and future powertrain technologies and trends in 2020. *Transportation Engineering*, 5, 100080.

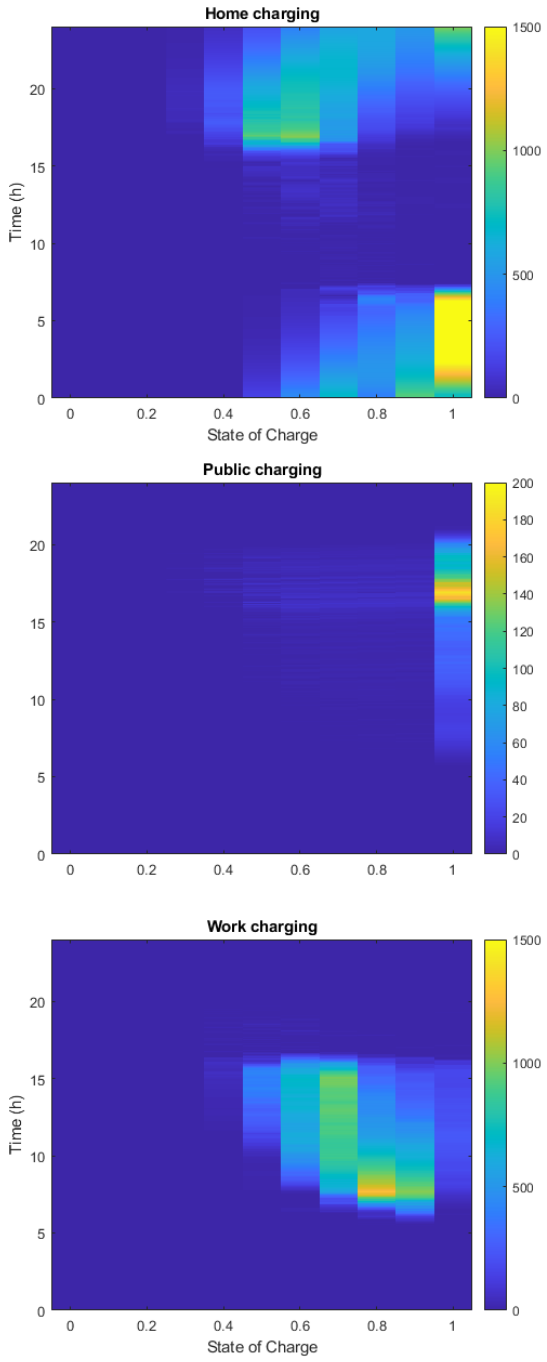

Fig. 4. Distribution of EVs according to their SoC at each charging station over time in the coordinated charging case. Brighter colours indicate more present EVs at that SoC. Note the different color scale in case of public charging station.

European Commission and Directorate-General for Energy (2019). *Effect of electromobility on the power system and the integration of RES : study S13*. Publications Office. doi:doi/10.2833/12919.

Fernandez, L.P., San Román, T.G., Cossent, R., Domingo, C.M., and Frias, P. (2010). Assessment of the impact of plug-in electric vehicles on distribution networks. *IEEE transactions on power systems*, 26(1), 206–213.

Henry, R. and Ernst, D. (2021). Gym-ANM: Reinforcement learning environments for active network management tasks in electricity distribution systems. *Energy and AI*, 5, 100092.

López, M., Martin, S., Aguado, J., and de la Torre, S. (2013). V2g strategies for congestion management in microgrids with high penetration of electric vehicles. *Electric Power Systems Research*, 104, 28 – 34. doi: 10.1016/j.epsr.2013.06.005.

Morlock, F., Rolle, B., Bauer, M., and Sawodny, O. (2019). Forecasts of electric vehicle energy consumption based on characteristic speed profiles and real-time traffic data. *IEEE Transactions on Vehicular Technology*, 69(2), 1404–1418.

Tinney, W. and Hart, C. (1967). Power flow solution by newton's method. *IEEE Transactions on Power Apparatus and Systems*, PAS(86), 1449–1460.

Wenzel, G., Negrete-Pincetic, M., Olivares, D.E., MacDonald, J., and Callaway, D.S. (2017). Real-time charging strategies for an electric vehicle aggregator to provide ancillary services. *IEEE Transactions on Smart Grid*, 9(5), 5141–5151.

Zhou, Z., Zhang, X., Guo, Q., and Sun, H. (2021). Analyzing power and dynamic traffic flows in coupled power and transportation networks. *Renewable and Sustainable Energy Reviews*, 135, 110083.

Zimmerman, R.D., Murillo-Sánchez, C.E., and Thomas, R.J. (2011). Matpower: Steady-state operations, planning, and analysis tools for power systems research and education. *IEEE Transactions on Power Systems*, 26(1), 12–19. doi:10.1109/TPWRS.2010.2051168.